Journal of Manufacturing Processes
Vol. 7/No. 2
2005

FEM-Based Process Design for Laser Forming of Doubly Curved Shapes

Chao Liu and **Y. Lawrence Yao,** Dept. of Mechanical Engineering, Columbia University, New York, New York, USA

Abstract

This study presents a finite element method (FEM) based three-dimensional laser forming process design methodology for thin plates to determine the laser scanning paths and heating conditions. The strain fields were first calculated via FEM. The laser scanning paths were chosen perpendicular to the averaged principal minimum strain direction. The ratios of in-plane and bending strain were calculated to help determine the heating condition. Two typical doubly curved shapes—a pillow shape and a saddle shape—were studied, and the overall methodology was validated by experiments.

Keywords: *Laser Forming, Process Design, Sheet Metal, Doubly Curved Shapes, Finite Element Method*

1. Introduction

Significant progress has been made in analyzing and predicting laser forming processes of sheet metal. To advance the process further for realistic forming applications in an industrial setting, it is necessary to consider the issue of process design, which is concerned with determination of laser scanning paths and heating conditions given a desired shape to form.

A number of approaches have been attempted in the past few years in laser forming process design. Genetic algorithm based design (Shimizu 1997; Cheng and Yao 2001) and response surface methodology based robust design (Liu and Yao 2002) have been reported. They are either for 3-D shapes with significantly simplified design tasks or for quasi 3-D shapes such as cylindrical shapes and axisymmetrical shapes. However, these methods are not appropriate for general 3-D process design of doubly curved shapes due to their geometry complexity.

In a series of reports, Ueda et al. (1994a,b,c) addressed issues in the development of a computer-aided process planning system for plate bending by line heating. In the first report, the concept of inherent strain was emphasized, but its significance was not adequately articulated or demonstrated. Scanning paths were determined based on FEM-determined in-plane strain, and heating condition determination was not addressed. This approach is not directly applicable to laser forming process design because no consideration for the characteristics of the laser forming process was given. The second report examined forming procedures for three simple curved shapes often encountered in shipyards. The prediction was found to be in agreement with the real practice of skilled workers. However, the approach too heavily relied on prior experience. Moreover, when bending strain is relatively large, a mechanical means such as a rolling machine was used to generate the bending strain, which is not suitable for an automatic laser forming process.

Jang and Moon (1998) developed an algorithm to determine the heating lines based on the lines of curvature of a design surface and the extrema of principal curvatures along them. This method, however, may only work for simple surfaces. Heating condition, such as power and speed of the heat source, also has not been addressed. Edwardson et al. (2001) and Watkins et al. (2001) aimed to establish rules for positioning and sequencing the scanning paths required for the 3-D laser forming of a saddle shape from rectangular sheet material. Various scanning patterns were first postulated and then modeled via FEM. However, the work too heavily relied on prior experience in coming up with the patterns in the first place and may become even less effective when the shapes to be formed become more complex. Furthermore, a constant scanning speed was assumed throughout an entire scanning pattern of a shape, and this severely limits the realization of the full process capability of laser forming.

Cheng and Yao (2004) presented a methodology to design laser scanning paths and heating conditions of laser forming for a general class of 3-D shapes from thin sheet metal. The strain field was calculated by FEM. In determining laser scanning paths and heating conditions, however, this method

This paper is an expanded version of a paper published in the *Transactions of NAMRI/SME*, Vol. 31, 2003.

only considered the in-plane component of the total strain and, therefore, may incur larger errors for thicker plates. Liu, Yao, and Srinivasan (2004) proposed strategies for solving essentially the same process design problem as above. The strain field was determined based on differential geometry and an optimization approach. This method, however, concerned the middle surface only, again neglecting the effect of bending strains across the thickness of a plate, and the method therefore only worked well for very thin plates.

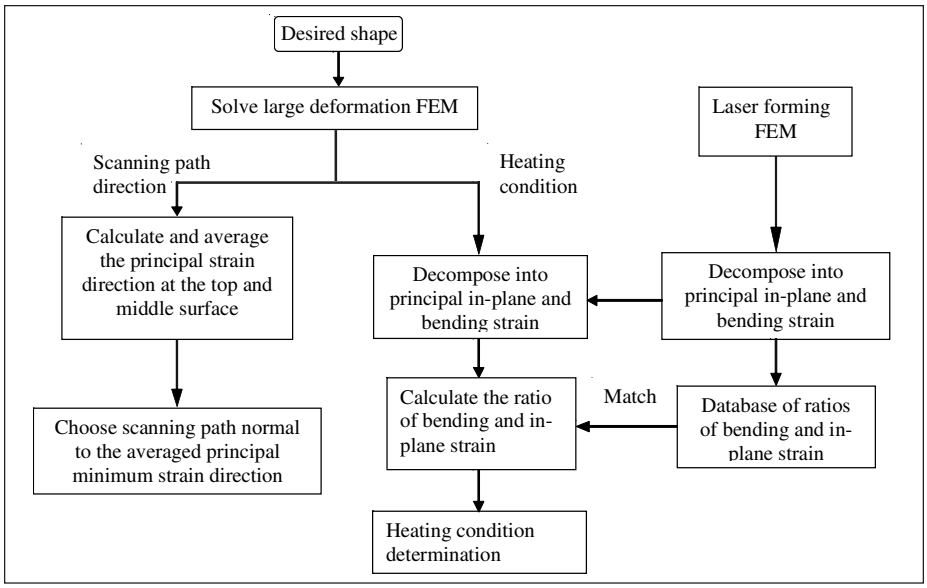

Figure 1
Flow Chart of Laser Forming Process Design

This study presents an FEM-based 3-D laser forming process design method, which extends the method's applicability to relatively thicker plates by considering bending strain in addition to in-plane strain. The strain field was calculated by way of an elastic, large-deformation FEM model; the rationale of using the elastic model is given later in the paper. The laser scanning paths were chosen taking into account the principal minimum strain direction of both the top surface and the middle surface of a plate. The ratios of in-plane and bending strain were calculated to help determine the heating condition. Two typical doubly curved shapes were studied, and the overall methodology was validated by experiments.

2. Problem Description

The flexural properties of a plate depend greatly on its thickness in comparison with other dimensions. A thin plate normally has a ratio of $10 < a/h < 100$, where h is a plate thickness and a is a typical dimension of a plate (Ventsel and Krauthammer 2001). In this study, the ratios a/h of the desired shape range from 16 to 89 (thickness ranges from 0.89 mm to 5 mm; width and length are both 80 mm), as opposed to about 123 in Cheng and Yao (2004) and about 90 in Liu, Yao, and Srinivasan (2004). Although thin-plate theories are still applicable in the present study, additional considerations, especially for bending strains, need to be given.

The overall design strategy is outlined in *Figure 1*. First, a strain field is obtained via a large-deformation, elastic FEM by flattening the desired shape. A large-deformation model is used because the desired shape has a large deflection relative to its thickness. The elastic FEM is utilized because strain-field development from the desired shape to planar shape is primarily geometrical and it simplifies the computation without altering the problem. This point will be elaborated on in section 3.1. After obtaining the strain field, the principal minimum strains and directions in both the middle and top surfaces are calculated by solving the eigenvalues and eigenvectors of the strain tensor. Because in the laser forming process the highest compressive strains occur in the direction perpendicular to a scanning path, it is natural to place a laser path perpendicular to the principal minimum strain direction. In this study, scanning paths are chosen to be perpendicular to the averaged minimal principal strain directions between top and middle surfaces.

Different from forming a singly curved shape, forming a doubly curved shape requires not only bending strains (angular distortion) but also in-plane strains (stretching/contraction of the middle surface of a plate). Therefore, at each material point in the plate, the principal minimum strain can be decomposed into in-plane strain and bending strain components. To match the required strain field in a laser

forming process, not only did the principal minimum strain in the middle surface need to be satisfied, but also the strains across the thickness, namely, the distribution of bending strain. Therefore, the introduction of ratio of in-plane strain with bending strain characterizes the nature of strains not only in the middle surface but also all across the thickness of the plate. For a specific principal minimum strain, there exist multiple heating conditions (different combinations of laser power, velocities, and so on). However, among them, only one satisfies both of in-plane and bending strain across the thickness. It is important to determine heating conditions (that is, laser power P and scanning speed V) of a laser forming process such that not only the total strain at each point but also the ratio between the in-plane and bending strains are realized. This is possible because a strain field generated by the laser forming process has its own characteristics; such characteristics may vary even under the same line-energy input level (that is, the same P/V ratio) and, therefore, provide the possibility of matching the desired strains and ratio. To get more understanding on the strain field generated by the laser forming, once again the FEM is utilized. A database of laser forming FEM results based on the simplest straight scan, but under a variety of conditions and validated experimentally, is established to aid the heat condition determination. To match the required strain field, not only did the principal minimum strain in the middle surface need to be satisfied, but also the strains across the thickness. Therefore, the introduction of the ratio of in-plane strain to bending strain characterizes the nature of strains not only in the middle surface, but also all across the thickness of the plate.

Surfaces of many engineering structures are commonly fabricated as doubly curved shapes to fulfill hydrodynamic, aesthetic, or structural functional requirements. In this study, two distinctive doubly curved surfaces are chosen as desired shapes in this study. They are a pillow shape, which has positive Gaussian curvature over the entire surface, and a saddle shape, which has negative Gaussian curvature over the entire surface. The two shapes are specified by a cubic-spline cross section sweeping along a path of a cubic-spline curve. The sweep surface is defined by: $S(x,y) = A(x) + B(y)$, $x,y \in [0,80]$ in mm. For the pillow shape, $A(x)$ is defined by (0,0,0), (40,0,1.7), and (80,0,0), and $B(y)$ is defined by (0,0,0), (0,40,2.9), and (0,80,0). For the saddle shape, $A(x)$ is defined by (0,0,0), (40,0,1.95), and (80,0,0), and $B(y)$ is defined by (0,0,0), (0,40,–1.95) and (0,80,0). The adjacent sides of the pillow shape are not identical, with the one along the x direction curving slightly higher. The saddle shape bends up at a pair of opposite sides and down at the other pair with the same magnitude. The desired shapes are shown in *Figures 2a* and *2b*, respectively.

3. Strain Field Attainment

As indicated in the previous section, the first step in the laser forming process design is to determine the strain field required to form into the desired shape. The strain field of the planar development is solved by a large elastic deformation FEM model under displacement constraints. The desired shape is placed

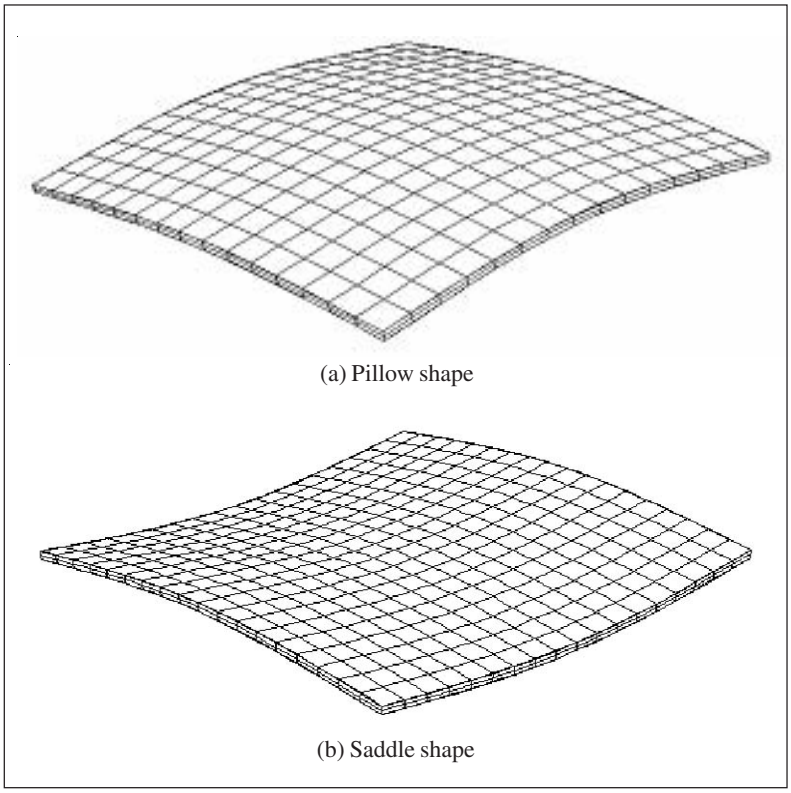

Figure 2
Doubly Curved Shapes To Be Laser Formed (80 × 80 × 1.4 mm)

between two flat rigid bodies and compressed into a planar shape to generate the strain field. The top rigid body is given a step-by-step displacement toward the bottom one along the thickness directions until the gap between them is equal to the thickness of the desired shape. It is assumed that there is no friction between the rigid bodies and the desired shape.

The development of a strain field from one shape to another is primarily a geometrical problem and is independent of material properties. In fact, it has been shown that the strain field determination is independent of Young's modulus (Cheng and Yao 2004). Elastic FEM is used instead of elastic/plastic FEM for this geometrical step because less material properties need to be specified in elastic FEM. The large-deformation model is employed for the following reasons. In the case of small deflection, the normal displacement component of the midplane (w_0) is small compared with the plate thickness (h), and thus the in-plane strain can be neglected. However, if the magnitude of deflection increases beyond a certain level ($w_0 > 0.3h$), these deflections are accompanied by stretching or contraction of the midplane and therefore cannot be neglected (Ventsel and Krauthammer 2001). In this study, the ratio w_0/h reaches 3.3 and, therefore, large-deformation FEM is necessary. In addition, as discussed in section 2, the sheet thickness dealt with in the paper falls within the usual definition of thin plates although the bending strain cannot be neglected.

The governing relations for elastic large deformation of a thin plate are briefly summarized. It is assumed that the material of the plate is elastic, homogenous, and isotropic; the straight lines, initially normal to the middle surface before bending, remain straight and normal to the middle surface during the deformation, and the length of such element is not altered. Deflection w_0 in the z (thickness) direction is assumed large relative to the thickness h of the plate, and therefore, membrane forces (N_x, N_y, and N_{xy}) become more pronounced. In the middle surface, the strain-displacement equations can be expressed as (Ventsel and Krauthammer 2001):

$$\varepsilon_{xx}^0 = \frac{\partial u_0}{\partial x} + \frac{1}{2}\left(\frac{\partial w_0}{\partial x}\right)^2,\ \varepsilon_{yy}^0 = \frac{\partial v_0}{\partial x} + \frac{1}{2}\left(\frac{\partial w_0}{\partial y}\right)^2,$$
$$\gamma_{xy}^0 = \frac{\partial u_0}{\partial y} + \frac{\partial v_0}{\partial x} + \frac{\partial w_0}{\partial x}\frac{\partial w_0}{\partial y} \tag{1}$$

where u_0, v_0, and w_0 are the displacement components, and ε_{xx}^0, ε_{yy}^0, and γ_{xy}^0 are the strains at the middle surface, respectively. The total strains in the layer of the plate parallel and a distance z from the middle surface can be written as

$$\varepsilon_{xx} = \varepsilon_{xx}^0 - \frac{\partial^2 w_0}{\partial x^2} z,\ \varepsilon_{yy} = \varepsilon_{yy}^0 - \frac{\partial^2 w_0}{\partial y^2} z,$$
$$\gamma_{xy} = \gamma_{xy}^0 - 2\frac{\partial^2 w_0}{\partial x \partial y} z \tag{2}$$

The equilibrium equation for the large-deflection plate analysis follows Hookes law and can be expressed as

$$\frac{1}{Eh}\left[\frac{\partial^2}{\partial y^2}\left(N_x - \nu N_y\right) + \frac{\partial^2}{\partial x^2}\left(N_y - \nu N_x\right) - 2\left(1+\nu\right)\frac{\partial^2 N_{xy}}{\partial x \partial y}\right]$$
$$= \left(\frac{\partial^2 w_0}{\partial x \partial y}\right)^2 - \frac{\partial^2 w_0}{\partial x^2}\frac{\partial^2 w_0}{\partial y^2} \tag{3}$$

where $\varepsilon_{xx}^0 = \frac{1}{Eh}\left(N_x - \nu N_y\right)$, $\varepsilon_{yy}^0 = \frac{1}{Eh}\left(N_y - \nu N_x\right)$, and $\gamma_{xy}^0 = \frac{N_{xy}}{Gh}$; E and G are Young's modulus and shear modulus, respectively, and ν is Poisson's ratio.

The strains, membrane forces, and displacement, w_0, can be solved by the above set of equations, yielding two governing differential equations:

$$\frac{\partial^4 \varphi}{\partial x^4} + 2\frac{\partial^4 \varphi}{\partial x^2 \partial y^2} + \frac{\partial^4 \varphi}{\partial y^4} = h\left[\left(\frac{\partial^2 w_0}{\partial x \partial y}\right)^2 - \frac{\partial^2 w_0}{\partial x^2}\frac{\partial^2 w_0}{\partial y^2}\right] \tag{4}$$

$$\frac{\partial^4 w_0}{\partial x^4} + 2\frac{\partial^4 w_0}{\partial x^2 \partial y^2} + \frac{\partial^4 w_0}{\partial y^4}$$
$$= \frac{1}{D'}\left[P' + \frac{\partial^2 \varphi}{\partial y^2}\frac{\partial^2 w_0}{\partial x^2} + \frac{\partial^2 \varphi}{\partial x^2}\frac{\partial^2 w_0}{\partial y^2} - 2\frac{\partial^2 \varphi}{\partial x \partial y}\frac{\partial^2 w_0}{\partial x \partial y}\right] \tag{5}$$

where $D' = \frac{h^3}{12(1-\nu^2)}$, $N_x = \frac{\partial^2 \phi}{\partial y^2}$, $N_y = \frac{\partial^2 \phi}{\partial x^2}$, $N_{xy} = -\frac{\partial^2 \phi}{\partial x \partial y}$, $\varphi = \phi / E$, and $P'(x,y)$ is the lateral load in the z direction $P(x,y)$ divided by E.

Once a desired shape is given, that is, deflection w_0 and curvatures $\frac{\partial^2 w_0}{\partial x^2}$, $\frac{\partial^2 w_0}{\partial y^2}$, and $\frac{\partial^2 w_0}{\partial x \partial y}$ are known,

φ and P' and, in turn, the in-plane strains, ε^0_{xx}, ε^0_{yy}, and γ^0_{xy} can be calculated under appropriate boundary conditions, and the calculation is independent of Young's modulus. However, Eq. (3) indicates that ε^0_{xx}, ε^0_{yy}, and γ^0_{xy} depend on Poisson's ratio ν, which is a geometric parameter. The total strain ε_{xx}, ε_{yy}, and γ_{xy} can also be calculated [Eq. (2)]. The FEM model was implemented in ABAQUS.

3.1 Decomposition of Strains

The above formulation assumes thin plates and therefore involves only ε_{xx}, ε_{yy}, and γ_{xy}, while the FEM implementation gives 3-D strains in terms of tensor. To obtain principal strains and bending strains directly from the tensor $\boldsymbol{E}$, the steps are briefly outlined below. $\boldsymbol{E}$ can be expressed in terms of $\varepsilon_1 \boldsymbol{n}_1 \boldsymbol{n}_1^{\mathrm{T}} + \varepsilon_2 \boldsymbol{n}_2 \boldsymbol{n}_2^{\mathrm{T}} + \varepsilon_3 \boldsymbol{n}_3 \boldsymbol{n}_3^{\mathrm{T}}$, where principal strains, ε_1, ε_2, and ε_3 $\left(\varepsilon_1 \le \varepsilon_2 \le \varepsilon_3\right)$, and the orientation of the principal strain, $\boldsymbol{n}_1$, $\boldsymbol{n}_2$, and $\boldsymbol{n}_3$, correspond to the eigenvalues and eigenvectors of the strain tensor $\boldsymbol{E}$ at that material point. Therefore, ε_1, ε_2, and ε_3, and $\boldsymbol{n}_1$, $\boldsymbol{n}_2$, and $\boldsymbol{n}_3$ can be obtained by solving the eigenvalue problem

$$\boldsymbol{En} = \varepsilon \boldsymbol{n} \tag{6}$$

where ε and $\boldsymbol{n}$ are principal strain and corresponding principal strain direction, respectively. *Figure 3* shows the contour plots of the minimal principal strain $\left(\varepsilon^0_1\right)$ distribution in the middle surface of the desired shape obtained from the FEM model. In a thin plate, the variation of strain across the thickness is assumed to be linearly distributed [Eq. (2)]; therefore, the strain in the middle of the plate can be taken as the in-plane strain. As seen, the strain field of the pillow shape shown in *Figure 3a* is only symmetrical about the *x* and *y* axes, while the strain field of the saddle shape is symmetric about the origin. This is obviously because the pillow shape specified in section 2 is not symmetric about the origin.

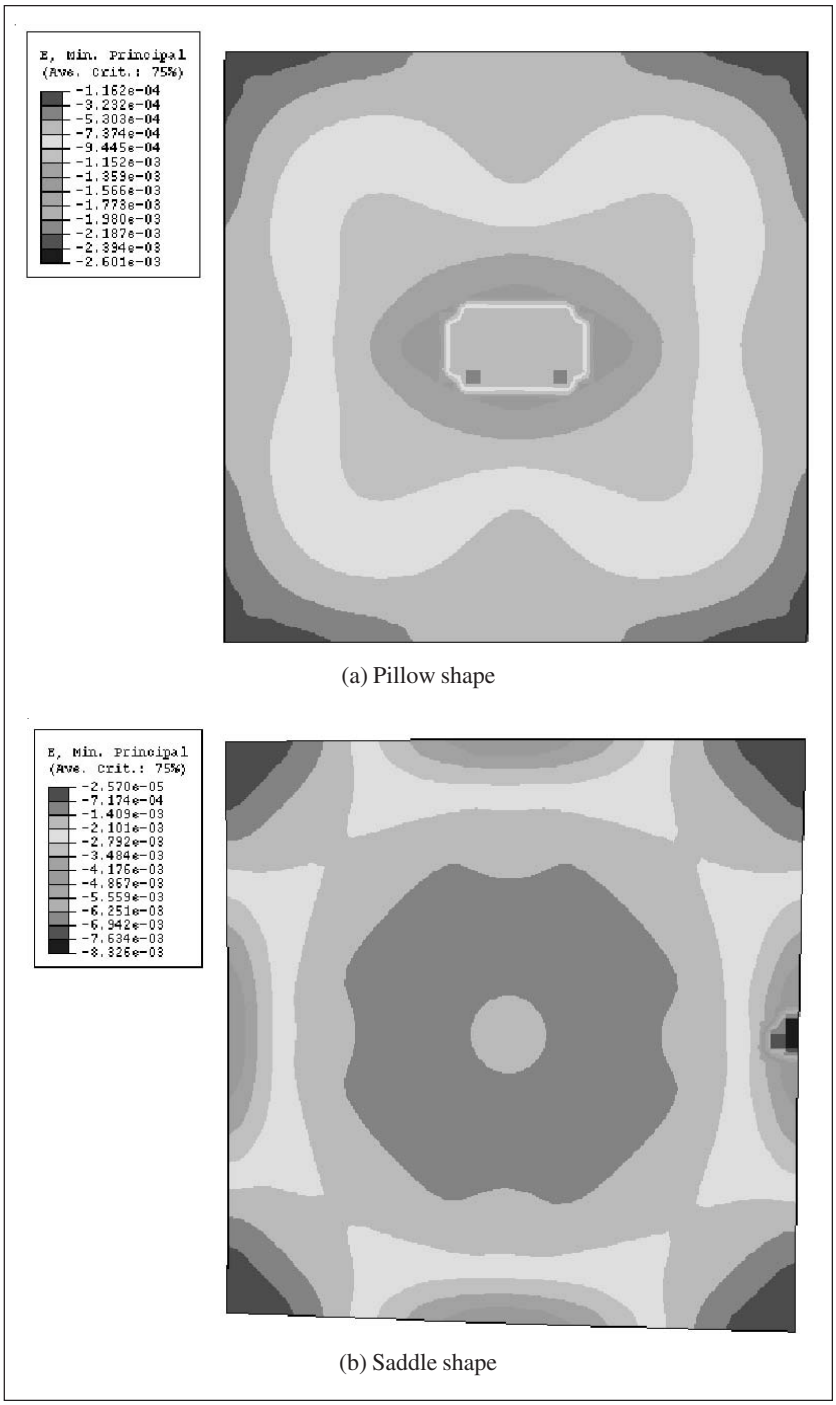

(a) Pillow shape

(b) Saddle shape

Figure 3
Minimum Principal Strain in Middle Surface (80 × 80 × 1.4 mm)

Figures 4a through *4d* show the magnitude and orientation of minimum principal strain at the middle surface and top surface of both pillow and saddle shapes. The length of a bar in the plots represents the magnitude of minimum principal strain at that location. These strains represent the required strain

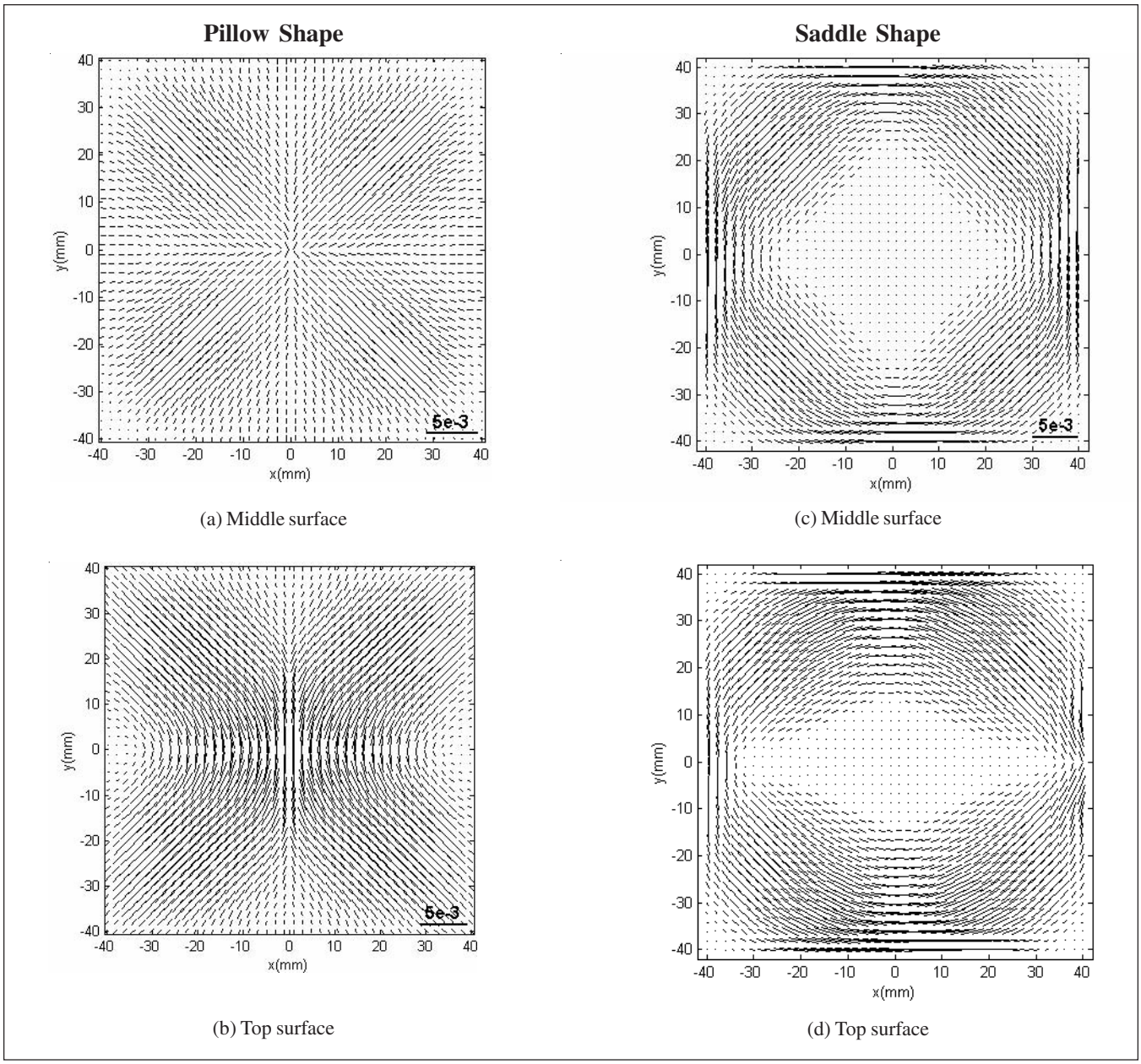

Figure 4
Vector Plots of Minimum Principal Strain at (a) Middle Surface and (b) Top Surface of Pillow Shape, and (c) Middle Surface and (d) Top Surface of Saddle Shape. (Length represents strain magnitude; orientation represents strain direction.)

field to be realized by the laser forming process at these planes. Clearly, the minimum principal strain (ε_1) and direction ($\boldsymbol{n}_1$) at a physical location represents the magnitude and direction, respectively, of maximum shrinkage at that point.

The bending strain is caused by the nonuniform distribution of strain in the thickness direction. Given an (x, y) location, the bending strain at that location varies along the thickness direction and is generally defined as the difference between strain at that z value and the strain at the mid-plane of the sheet. For a thin plate, the bending strain linearly increases with thickness and reaches the maximal value at sheet surfaces [Eq. (2)]. The minimal principal bending strain at the top surface ($z = h/2$) is calculated based on the minimal principal strains found above.

$$\boldsymbol{\varepsilon}_b = \varepsilon_1^{h/2}\boldsymbol{n}_1^{h/2} - \varepsilon_1^{0}\boldsymbol{n}_1^{0} \tag{7}$$

where $\varepsilon_1^{h/2}$ and $\boldsymbol{n}_1^{h/2}$ are magnitude and direction of

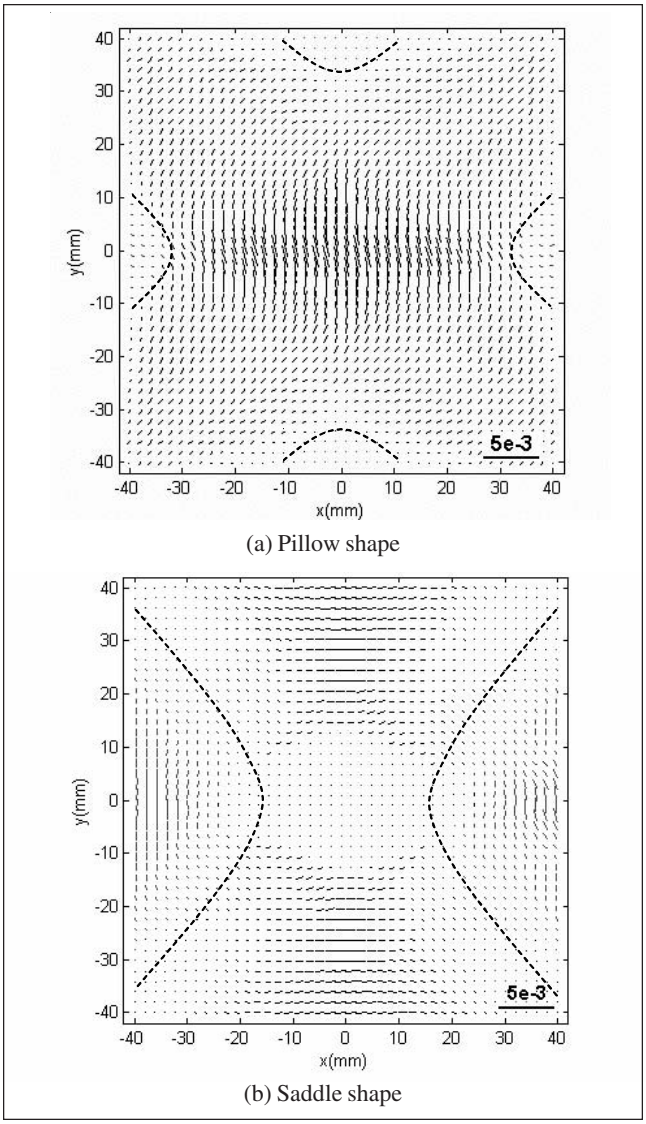

Figure 5
Vector Plots of Bending Strain

the principal minimum strain at z, and ε_1^0 and $\boldsymbol{n}_1^0$ are magnitude and direction of the principal minimum strain at the mid plane. *Figures 5a* and *5b* show the magnitude and orientation of the minimal principal bending strain at the top surface of the pillow shape and the saddle shape, respectively. The length of a bar in the plots represents the magnitude of bending strain at that location. The regions within the dashed lines (also in red) represent positive bending strain, while the rest of areas represent negative bending strains. The physical meaning of negative bending strain is that the top surface is subject to more compressive strain than the middle. In the laser forming process operating under a temperature-gradient mechanism, the plate bends toward the laser beam.

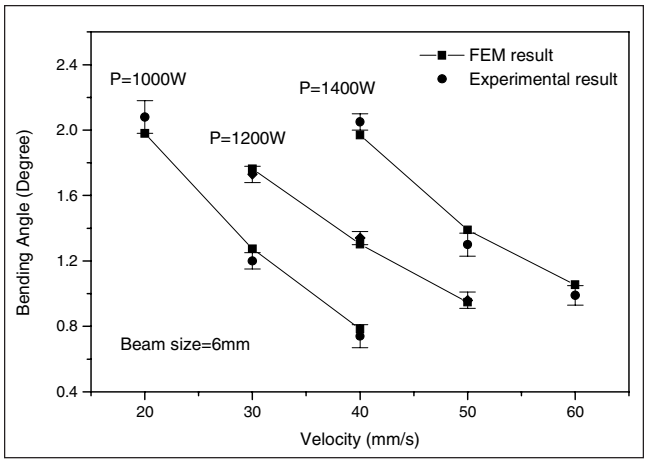

Figure 6
Experimental Validation of Numerically Determined Bending Angle. (Error bars represent standard deviation of two samples.)

This indicates that the laser should be placed on the top surface of the plate for this case. If the positive bending strains are much smaller than the negative ones and occur in much smaller regions, they therefore may be neglected as in the case of the pillow shape, but not in the saddle case.

3.2 Laser Forming FEM

After analyzing the strain field on the mechanical pressing side, the strain field in the laser forming process needs to be explored as well. In an effort to establish a database about the characteristics of laser forming induced strain distribution under various heating conditions, a simple straight line scanning along a centerline of 80 × 80 × 1.4 mm plates is assumed in the FEM simulation of the laser forming process. Due to symmetry about the centerline, only half of the plate is simulated. The workpiece material is assumed isotropic. Material properties such as Young's modulus, yield stress, heat transfer properties, thermal conductivity, and specific heat are temperature dependent. The material is 1010 steel. The heat flux of the laser beam is assumed to follow a Gaussian distribution. No melting is involved and no external forces are applied in the forming process. The symmetric plane is assumed to be adiabatic. Commercial FEM software, ABAQUS, is used to solve the thermal mechanical problem. Liu and Yao (2002) give more details.

The simulation results have been validated by experiments, which will be described in more detail in a subsequent section. As shown in *Figure 6*, the bending angles calculated from FEM under various

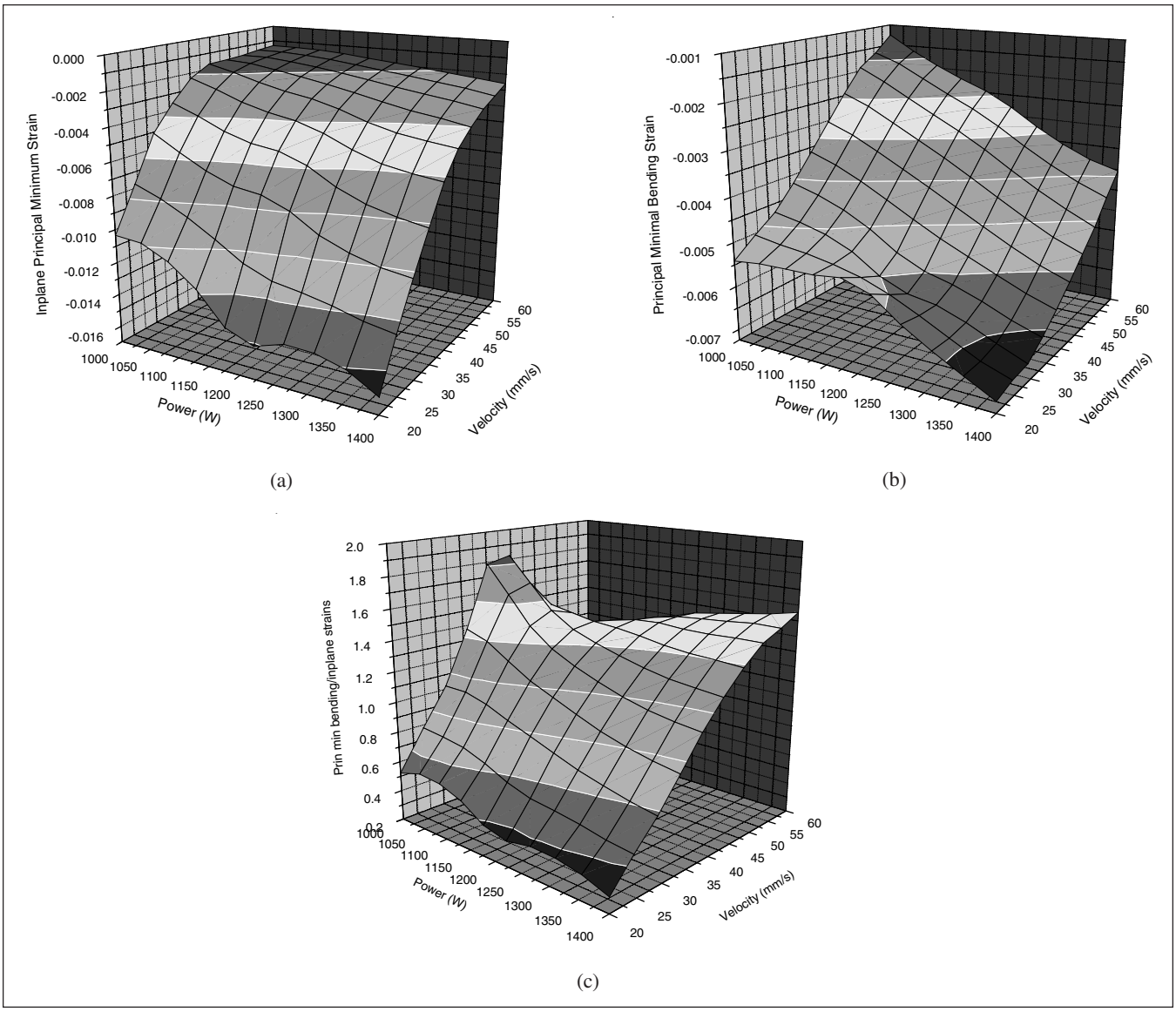

Figure 7
(a) Principal Minimum In-Plane Strain, (b) Principal Minimum Bending Strain, and (c) FEM Determined Ratio of Principal Minimum In-Plane Strain and Bending Strain (laser beam diameter is 6 mm)

conditions are within the experimental errors. A database of in-plane and bending principal minimum strains under these conditions is established as shown in *Figures 7a* and *7b*, respectively. *Figure 7c* shows the ratios between the in-plane and bending strains under these conditions. Obviously, many combinations of laser power, *P*, and scanning speed, *V*, will give an identical ratio. This is indicative of the feasibility to choose a combination that matches not only the ratio but also the in-plane and bending strain values required by forming a desired shape.

4. Scanning Path Determination

It has been discussed in the previous sections that the scanning path should be placed perpendicular to the minimum principal strain direction because it is well known that the maximal compression occurs in the direction perpendicular to a laser scanning path in laser forming. For a very thin plate where bending strains are small, the in-plane minimal principal strain direction, $\boldsymbol{n}_1^0$, should be used to determine the scanning paths (Cheng and Yao 2004). For the plates used in this study, there are sizable bending strains

in some regions of the plate (*Figure 5*), and it seems more reasonable to vector average the in-plane strain direction, $\boldsymbol{n}_1^0$, and the total strain direction, $\boldsymbol{n}_1^{h/2}$, at the top surface, where the highest bending strain is found, as the basis for the laser path planning. *Figures 8a* and *8b* show a quarter (due to symmetry) of the plate with averaged $\varepsilon_1^0 \boldsymbol{n}_1^0$ and $\varepsilon^{h/2}\boldsymbol{n}^{h/2}$, which is used for determining scanning path direction.

In determining the spacing of adjacent scanning paths, a number of guidelines are followed. In general, the smaller the spacing, the more precise the desired shape can be formed. Practically, however, the adjacent paths cannot be too close and also because being too close will violate the underlying assumption when using the laser forming FEM. The assumption is that adjacent paths should be independent with each other. The regions on a shape that have larger strains need to be scanned more and more exactly and therefore require denser paths. Roughly speaking, spacing between two adjacent paths, D_{paths}, should be equal to average strain generated by laser forming, $\varepsilon_{\text{laser}}$, multiplied by laser beam spot size, d_{laser}, and divided by the average principal minimal strain over the spacing. *Figures 8a* and *8b* shows scanning paths determined following these guidelines. As seen, they are perpendicular to the minimal principal strain directions everywhere and denser around the center of the quarter due to larger strains there. Heating conditions are also indicated along the paths; their determination will be explained in the next section.

Another consideration is which side of the plate should be scanned. The physical meaning of negative bending strain is that the top surface is subject to more compressive strain than the middle, which corresponds to a concave curvature in a given shape. In the laser forming process, the plate always bends toward the laser beam; therefore, the laser should be placed on the top surface of the plate where the bending strain is negative and be placed on the other side of the plate if the bending strains are positive. As shown from *Figure 5a*, the positive bending strains of the pillow shape are much smaller than the negative ones; because they are negligible, the laser should be scanned at top surface of the plate. On the other hand, the bending strains in the saddle shape reveal a different scenario. The positive bending strains and negatives strains are almost equally distributed, both in amount and magnitude. Therefore,

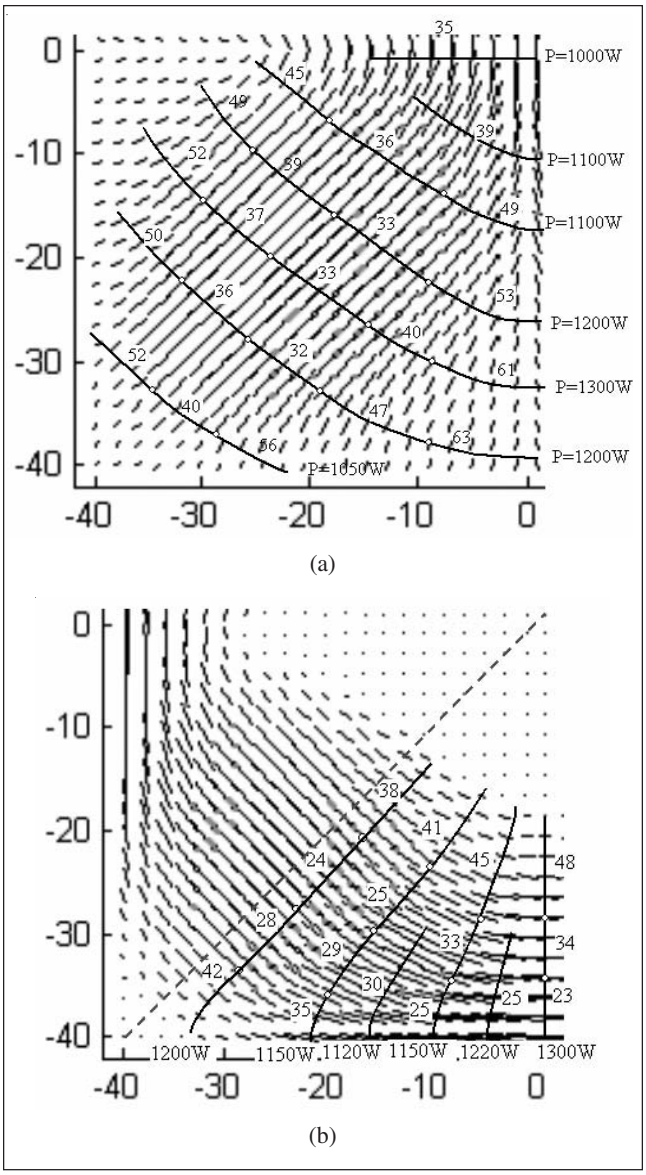

Figure 8
Laser Paths and Heating Conditions Determined for (a) Pillow Shape and (b) Saddle Shape. Only a quarter of the plate is shown due to symmetry. The strain field shown represents minimal principal in-plane strain averaged between top and middle surfaces (numbers next to segments on each scanning path represent scanning speed in mm/s).

it is necessary to place the laser path on both sides of the plate according to the distribution of the sign of the bending strain.

5. Heating Condition Determination

If the laser spot size is given, the heating conditions to be determined include laser power, *P*, and scanning velocity, *V*. While it is possible to continuously vary them to generate the strain field required

to form the desired shape, this study adopts the strategy of constant power and piecewise constant speed for a given path in favor of implementation simplicity. The procedure is summarized below. A path is broken down to a few segments such that within each segment the range of strain variation (highest minus lowest strain) is about the same as in other segments.

The segment having the largest strain, which has the strongest influence on the final shape, is first chosen. In determining the strain, strains between adjacent scanning paths are lumped together because all of these strains are to be imparted by the paths. The highest and lowest in-plane minimal principal strains in the segment is averaged and compared with those from the database established by the laser forming FEM, resulting in a group of (P,V) combinations. The process is repeated for the bending strains, resulting another group of (P,V) combinations. The intersection of these two groups gives a unique (P,V) combination for the segment. The determined P value is also adopted for the entire path. Ratios of principal minimum in-plane strains and bending strains versus laser power and velocity are calculated and plotted in *Figure 7c*. The magnitude of the ratio varies from 0.3 to 1.8. As indicated by the chart, heating conditions with lower velocities tend to have lower ratio numbers. This can be explained by the fact that, at lower speed level, more heat will be allowed to be dissipated and thus heat energy is more uniformly distributed across the thickness, and therefore, in-plane shrinkage will be dominant. On the other hand, the faster the speed, the less time allowed for heat to dissipate, the temperature gradient mechanism will be more pronounced, and bending strain will be more dominant.

To determine scanning speed, V, for another segment on the path, a level of compromise is needed because, with P chosen, to find a V value that satisfies the required ratio of in-plane and bending minimal principal strains (using *Figure 7*) as well as the strains themselves is generally unattainable. Assuming V^0 and V^1 are the scanning speeds determined by the in-plane strain, ε_1^0, and bending strain, $\varepsilon_1^{h/2}$, from the database, the scanning speed for the segment is

$$V = \frac{\varepsilon_1^0}{\varepsilon_1^0 + \varepsilon_1^1} V^0 + \frac{\varepsilon_1^1}{\varepsilon_1^0 + \varepsilon_1^1} V^1 \tag{8}$$

The procedure is repeated for other segments of the path as well as for all other paths. *Figures 8a* and *8b* shows the heating conditions determined following the above strategy. Due to symmetry, only one quarter of the plate is shown. As seen, a constant laser power is chosen for a path and a constant speed (unit: mm/s) for a segment. In the case of the saddle shape, both sides of the plate need to be scanned. Due to the geometric symmetry of the given shape, the heating conditions are kept the same on both sides of the plate. The region below in the dashed line (in red) needs to be scanned on the top side, while the region above the line is scanned on the other side, based on the explanations associated with *Figure 5*.

6. Experimental Validation

Experiments were conducted on 1010 steel coupons with dimensions 80 × 80 × 1.4 mm. The scanning paths and heating conditions in the experiments were determined as described above and indicated in *Figure 8*. The laser system used is a PRC-1500 CO_2 laser, which is capable of delivering 1,500 W laser power, and the laser beam diameter on the top surface of workpiece is 6 mm. The motion of workpieces was controlled by a Unidex MMI500 motion control system, which allows easy specifications of variable velocities along a path with smooth transitions from segment to segment.

Figure 9 shows the formed pillow and saddle shapes under these conditions. A coordinate measuring machine is used to measure the geometry of the formed shapes. *Figure 10* compares the geometry of the formed shape under the determined conditions and the desired shape. Only the top surface of the plate is measured and compared. A general agreement can be seen from the figure, and the middle of the plate shows some discrepancy. Pos-

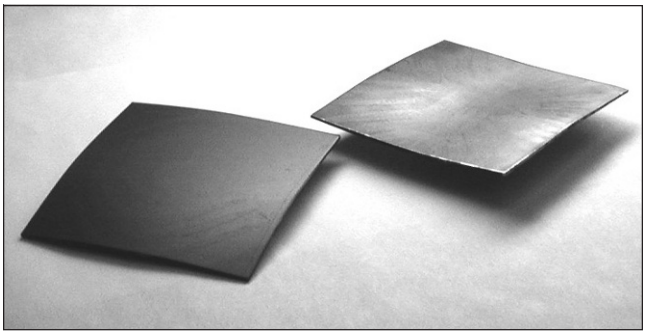

Figure 9
Laser-Formed AISI1010 Steel Plate Using Scanning Paths and Heating Condition Indicated in *Figure 8*

sible sources contributing to the discrepancy include the lumped method used to sum strains between adjacent paths; finite number of paths to approximate a continuous strain field; and constant power for each path and constant velocity for each segment. In forming the saddle shape, each side of the sheet metal is scanned alternatively, that is, scanning a path on a side, then scanning a path on the other side, and so on, to achieve the thermal symmetry to the maximal possible extent (Hennige 2000).

7. Further Discussion on Bending Strain and Thickness Effect

In the approach to obtain the bending strain presented in section 3.1, if the in-plane minimum principal strain has a similar direction as that at the top surface, the resultant bending strain has a similar direction as the in-plane strain such that there is no ambiguity to determine the direction of the scanning path. To guarantee that the bending strain and in-plane strain lie in the same direction, the bending strain is alternatively calculated as the appropriate strain in the bending strain tensor, projected along the minimum principal in-plane strain direction.

In a general 3-D space, the bending strain tensor is obtained by

$$\boldsymbol{E}_b = \boldsymbol{E}^1 - \boldsymbol{E}^0 \tag{9}$$

where $\boldsymbol{E}^1$ is the 3×3 strain tensor at the top surface and $\boldsymbol{E}^0$ is the 3×3 strain tensor in the middle surface. Once the minimum in-plane strain, $\varepsilon_1{}^0\boldsymbol{n}_1{}^0$, is obtained, the magnitude of the bending strain can be calculated as the following:

$$\varepsilon_b = n_1^0 \cdot E_b \cdot n_1^{0^T} \tag{10}$$

In this expression, ε_b is a scalar, with either positive or negative value, representing the magnitude of the bending strain whose direction is the same as $\boldsymbol{n}_1{}^0$. The expression of the bending strain can be simplified for the case of thin plates. Under the assumption of thin plate theory, the strain in the middle surface can be written as in Eq. (1), and the total strains in the layer of the plate parallel and a distance z from the middle surface can be written as in Eq. (2). As seen from Eq. (2), $\frac{\partial w_0}{\partial x}$ and $\frac{\partial w_0}{\partial y}$ represent the slope of the deformed shape in the x and y direction, and $\frac{\partial^2 w_0}{\partial x^2}$ and $\frac{\partial^2 w_0}{\partial y^2}$ are the local curvatures in the x and y direction. Therefore, the bending strain can be expressed by subtracting strain in the middle surface from the total strain, namely,

$$\boldsymbol{E}_b = \begin{pmatrix} -\frac{\partial^2 w_0}{\partial x^2} z & -\frac{\partial^2 w_0}{\partial x \partial y} z \\ -\frac{\partial^2 w_0}{\partial x \partial y} z & -\frac{\partial^2 w_0}{\partial y^2} z \end{pmatrix} \tag{11}$$

Figures 11a and *11b* show the magnitude and orientation of the bending strain obtained from Eq. (10), projected onto the *x*-*y* plane, for the pillow and saddle shapes, respectively. The length of a bar in the plots represents the magnitude of bending strain at that location. As seen in the plot, the bending strains are in the same direction as in-plane strain (*Figures 4a* and *4b*). In these plots, the red region represents positive bending strain, while the black region rep-

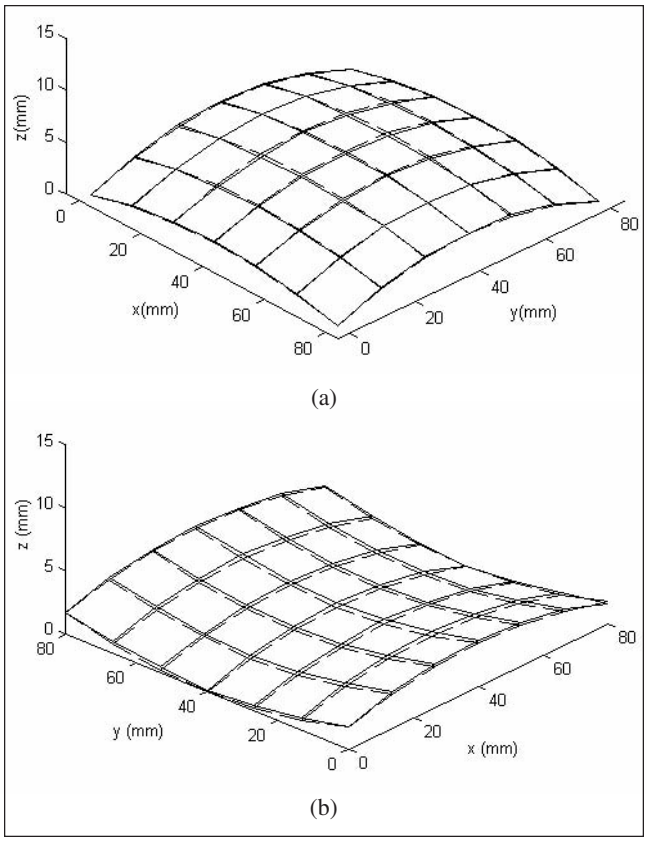

Figure 10
Comparison of Formed Shape (solid lines) and Desired Shape (dashed lines). Formed shape was measured by CMM.

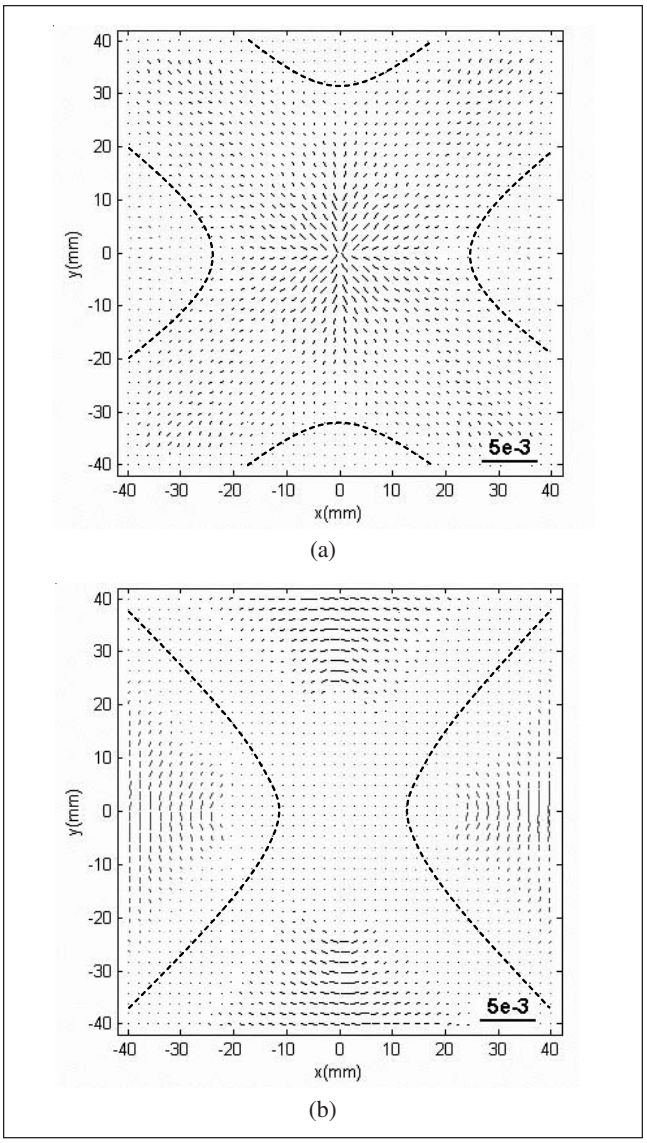

Figure 11
Vector Plot of Bending Strain of (a) Pillow Shape and (b) Saddle Shape Obtained Based on Eq. (10). (Plate thickness = 1.4 mm)

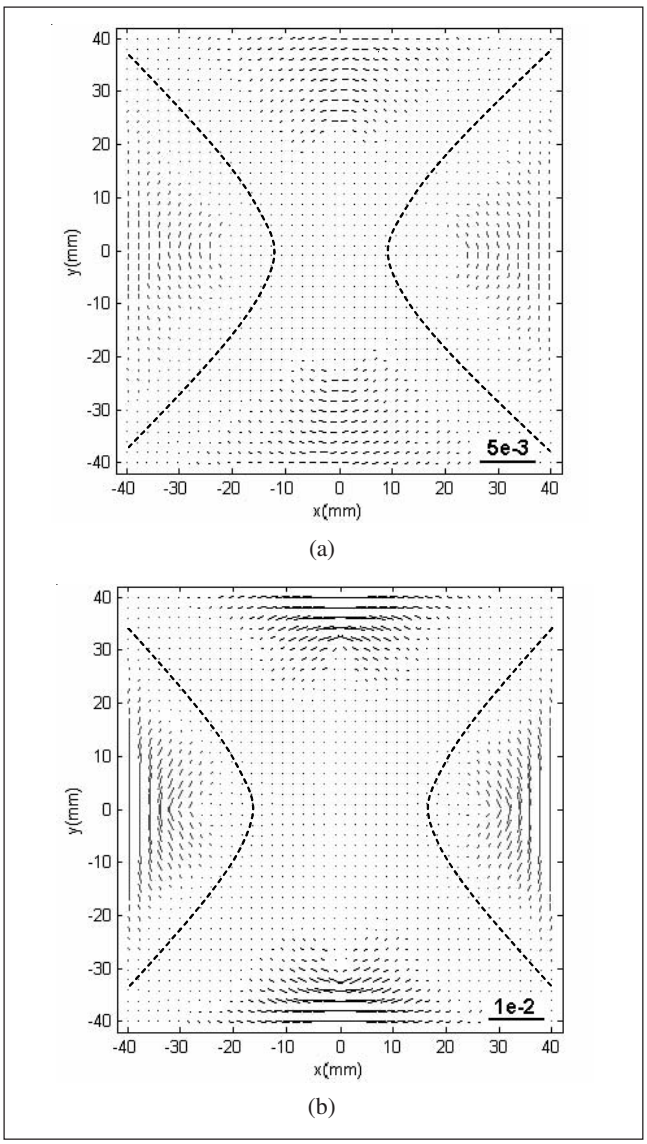

Figure 12
Vector Plot of Bending Strain of Saddle Shape with (a) 0.89 mm Thickness and (b) 5 mm Thickness. [Note: (b) scale is half of (a).]

resents the negative bending strain. The positive bending strain means that the strain is more compressive in the middle surface than the top surface, vice versa for the negative bending strain. Also worthy of mentioning is that the magnitude of the bending strain obtained based on Eq. (11) is almost identical to that obtained based on Eq. (10) and shown in *Figure 11*. Therefore, for a thin plate, it is adequate to use the plane strain formula [Eq. (11)] to obtain the bending strain.

As seen in Eq. (11), the magnitude of bending strain is proportional to the thickness of the plate. Therefore, whether a desired shape can be precisely formed or not depends on not only the given shape but also its thickness. The characteristics of in-plane strain and bending strain with various thicknesses were studied in this paper using two more thickness levels, 0.89 mm and 5 mm, in addition to the thickness 1.4 mm discussed so far for the saddle shape. The plate size remains the same as 80 × 80 mm. As expected, the magnitude and distribution of in-plane strains obtained for the 0.89 mm and 5 mm thick plates are essentially the same as that for the 1.4 mm plate shown in *Figure 4c*. However, this is not true for the bending strains. As shown in *Figures 12a* and *12b*, the magnitude of bending strain changed

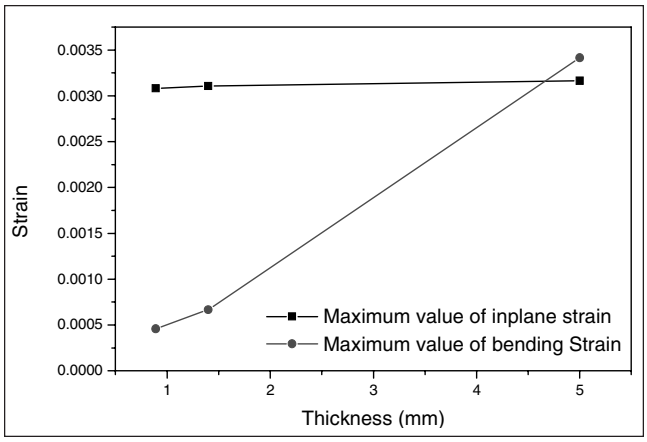

Figure 13
Variation of Maximum Value of Bending Strain and In-Plane Strain with Different Plate Thickness (from FEM simulation)

significantly as thickness changed. Compared with *Figure 11b* for the thickness of 1.4 mm, *Figure 12a* for the thickness of 0.89 mm shows smaller bending strains, while *Figure 12b* for the thickness of 5 mm shows much larger bending strain (note the scale here is halved for viewing clarity). The magnitude variation of the maximum value of bending strain and in-plane strain is plotted in *Figure 13*, which shows almost constant for the in-plane strain and almost linear change for the bending strain with thickness. This also means that when thickness changes one may need to change to a different beam spot size, or another laser forming mechanism such as a buckling mechanism, to obtain the required in-plane and bending strains for that thickness. For process design, this means that there might be a need to establish different databases for different plate thickness values.

8. Conclusions

The FEM-based 3-D laser forming process design methodology for thin plates considering the bending strain effect is experimentally shown effective. A strain field required to form a desired doubly curved shape is obtained through FEM first, decomposed to in-plane and bending strains, and both used to determine the scanning paths. An alternative way to obtain the bending strain is also presented. In determining heating conditions, the concept of in-plane and bending strain ratio is useful in approximately matching a strain distribution required to form a desired shape with that produced by a laser forming process.

References

Cheng, J. and Yao, Y.L. (2001). "Process synthesis of laser forming by genetic algorithms." *Proc.* of ICALEO 2001, Section D 604.

Cheng, J. and Yao, Y. (2004). "Process design of laser forming for three-dimensional thin plates." *ASME Trans., Journal of Mfg. Science and Engg.* (v126, n2), pp217-225.

Edwardson, S.P.; Watkins, K.G.; Dearden, G.; and Magee, J. (2001). "3D laser forming of saddle shape." *Proc.* of LANE 2001.

Hennige, T. (2000). "Development of irradiation strategies for 3D-laser forming." *Journal of Materials Processing Technology* (v103), pp102-108.

Jang, C.D. and Moon, S.C. (1998). "An algorithm to determine heating lines for plate forming by line heating method." *Journal of Ship Production* (v14, n4), pp238-245.

Liu, C. and Yao, Y.L. (2002). "Optimal and robust design of laser forming process." *Journal of Manufacturing Processes* (v4, n1), pp000-000.

Liu, C.; Yao, Y.L.; and Srinivasan,V. (2004). "Optimal process planning for laser forming of doubly curved shapes." *Trans. of ASME, Journal of Mfg. Science and Engg.* (v126, n1), pp1-9.

Shimizu, H. (1997). "A heating process algorithm for metal forming by a moving heat source." Master's thesis. Cambridge, MA: Massachusetts Institute of Technology.

Ueda, K.; Murakawa, H.; Rashwan, A.M.; Okumoto, Y.; and Kamichika, R. (1994a). "Development of computer-aided process planning system for plate bending by line heating (report 1) – relation between final form of plate and inherent strain." *Journal of Ship Production* (v10, n1), pp59-67.

Ueda, K.; Murakawa, H.; Rashwan, A.M.; Okumoto, Y.; and Kamichika, R. (1994b). "Development of computer-aided process planning system for plate bending by line heating (report 2) – practice for plate bending in shipyard viewed from aspect of inherent strain." *Journal of Ship Production* (v10, n4), pp239-247.

Ueda, K.; Murakawa, H.; Rashwan, A.M.; Okumoto, Y.; and Kamichika, R. (1994c). "Development of computer-aided process planning system for plate bending by line heating (report 3) – relation between heating condition and deformation." *Journal of Ship Production* (v10, n4), pp248-257.

Ventsel, E. and Krauthammer, T. (2001). *Thin Plates and Shells: Theory, Analysis and Applications*. New York: Marcel Dekker, Inc.

Watkins, K.G.; Edwardson, S.P.; Magee, J.; Dearden, G.; and French, P. (2001). "Laser forming of aerospace alloys." AeroSpace Mfg. Technology Conf.

Authors' Biographies

Chao Liu was a PhD candidate with the Dept. of Mechanical Engineering at Columbia University. His area of research interest includes optimal and robust process design methodologies as applied to laser forming processes.

Y. Lawrence Yao is a professor of mechanical engineering at Columbia University, where he directs the Manufacturing Research Laboratory. His area of research interests includes laser forming, laser peen forming, microscale laser shock peening, and laser micromachining. He has a PhD in mechanical engineering from the University of Wisconsin-Madison.